

Two fundamental constraints on the inner radii of accretion disks

ANDRZEJ A. ZDZIARSKI AND BARBARA DE MARCO¹

¹*Nicolaus Copernicus Astronomical Center, Polish Academy of Sciences, Bartycka 18, PL-00-716 Warszawa, Poland; aaz@camk.edu.pl, bdemarco@camk.edu.pl*

ABSTRACT

We have derived a method yielding very strong constraints on the inner radii of accretion disks in black-hole X-ray binaries based on the Stefan-Boltzmann law. It follows from considering the irradiating flux and the effective temperature of inner parts of the disk. Then, the presence of a quasi-thermal component with a color temperature higher than the effective one is required whenever Fe K fluorescence and reflection features are observed. The observed absence of such quasi-thermal components with the color temperature of ~ 1 keV rules out a disk extending close to the innermost stable circular orbit in high-luminosity hard states and requires it to be truncated, favoring the presence of a hot flow inside the disk truncation radius in those states. We have also derived a method based on comparing the disk densities fitted (by other authors) using high-density reflection codes with those calculated by us from the fitted ionization parameter, the source luminosity and the disk inner radius. However, we have found a very large scatter of the density ratios, preventing us from obtaining significant constraints as yet.

Keywords: accretion, accretion disks — black hole physics

1. INTRODUCTION

Hard X-ray spectra of hard-state black hole (BH) binaries and of many Seyfert active galactic nuclei (AGNs) are well described by thermal Comptonization in a hot plasma. However, the location of this plasma, either on the BH rotation axis, above the accretion disk, or within its inner truncation radius, has been a matter of intense debates (e.g., Kara et al. 2019; Mahmoud et al. 2019). Even in cases in which there is a consensus on the presence of a truncated disk, the value of the inner truncation radius, R_{in} , is not well determined. During quiescence of transient accreting BH binaries, $R_{\text{in}} \gtrsim 10^4 R_{\text{g}}$ (Dubus et al. 2001; Bernardini et al. 2016), where $R_{\text{g}} = GM/c^2$ is the gravitational radius and M is the BH mass. This implies the disk is also highly truncated during the initial phases of the outburst. However, we still do not know when the disk reaches the innermost stable circular orbit (ISCO), whether already in the hard state (e.g., García et al. 2015) or only during the transition to the soft state (e.g., Basak & Zdziarski 2016).

Here, we derive two sensitive tests of the accretion geometry, and the truncation radius in particular. The first is based on the basic physical constraint that the pure blackbody emission is the highest one achievable at a given source temperature (except for coherent radiation, which does not occur in hot conditions near accreting BHs). Since less effective thermalization results in the photon average energy higher than that of the blackbody, this sets a lower limit on the temperature of an irradiated disk, and, consequently, on R_{in} .

The second test follows from the X-ray reflection spectroscopy if both the ionization state of the reflector and its density can be determined. Since the ionization state depends primarily on the flux-to-density ratio, its fitted value together

with the density yields the irradiating flux measured at the source. If we also measure the observed flux and the distance to the source, this sets a constraint on the geometry of the source of primary X-rays and the reflector.

2. THERMALIZED REEMISSION

A major constraint on the source geometry in the hard state follows from considering the flux irradiating the cold medium in the system, F_{irr} (energy-integrated and per unit area). That flux is partly Compton-reflected, and partly absorbed and then reemitted. If that reemission would perfectly thermalize, it would appear as a blackbody at the effective temperature corresponding to the absorbed flux. However, the reprocessing does not lead to the full thermodynamic equilibrium, and the reemitted spectrum consists of many lines and edges on top of a quasi-thermal continuum (García et al. 2016). Still, we have a strict lower limit on the shape of the reemitted spectrum: its average energy has to be above the average energy of the blackbody at the effective temperature, T_{eff} , given by the Stefan-Boltzmann law,

$$\sigma T_{\text{eff}}^4 = (1 - a)F_{\text{irr}} + F_{\text{intr}}, \quad (1)$$

where σ is the Stefan-Boltzmann constant, a is the albedo and F_{intr} is the flux generated by an internal dissipation. The observed spectrum can be characterized by a color temperature, $T_{\text{col}} = \kappa T_{\text{eff}}$. In the case of intrinsic dissipation in disks of stellar-mass binaries, κ has been found to be in the range of ≈ 1.5 – 2 (Shimura & Takahara 1995; Davis et al. 2005).

We can estimate the irradiating flux if we know the observed bolometric flux of the primary source (e.g., due to Comptonization), $F_{\text{obs},0}$, the distance to the source, D , and its characteristic size scale, R . Assuming isotropy, the pri-

mary source luminosity, L_0 , equals $4\pi D^2 F_{\text{obs},0}$. We initially consider a simple planar geometry with the primary source on each side of the disk emitting $L_0/2$ away from the disk and $L_0/2$ toward it (thus, the total luminosity is $L = 2L_0$). The emission toward the disk is either Compton back-scattered or absorbed and reemitted, and each side of the disk emits in steady state $L_0/2$. The flux irradiating the disk can be written as $F_{\text{irr}} = L_0/(\zeta R^2)$, where ζ is a geometry-dependent factor. For example, for two isotropic point sources (‘lampposts’) irradiating the disk at the distance R at an angle θ between the ray and the disk normal, $\zeta = 2\pi/\cos\theta$. For an isotropic corona above and below a narrow ring between the inner radius R and $R + \Delta R$, $\zeta \approx 4\pi\Delta R/R$. Then we consider a radially-stratified isotropic and optically-thin corona above and below the disk. The irradiating flux at the inner radius, R_{in} , is

$$F_{\text{irr}}(R_{\text{in}}) = \frac{4\pi D^2 F_{\text{obs},0}}{\zeta R_{\text{in}}^2}, \quad (2)$$

where $\zeta = 2\pi$ for the standard radial dissipation profile $\propto R^{-3}$. From this, we can calculate $T_{\text{eff,in}} \equiv T_{\text{eff}}(R_{\text{in}})$.

These estimates are modified by GR, e.g., radiation of a lamppost on the rotation axis of the BH is focused toward both the disk and the horizon. Here we provide only approximate estimates and neglect this modification. The modification for scattering of the reflected emission in the corona (Steiner et al. 2017) can be partly accounted for by using the reflection fraction, \mathcal{R} . Furthermore, the geometry can be different from either disk corona or lamppost. In particular, if the disk (with a corona) is truncated at a $R_{\text{in}} > R_{\text{ISCO}}$, it is very likely that the flow below R_{in} is dissipative and hot, e.g., Yuan & Narayan (2014). Then the irradiating flux will be lower than that estimated above, and the observed \mathcal{R} will follow from the fraction of the emission still taking place in the corona, as well as by scattering and the geometry.

We now test the above constraint in the case of a luminous occurrence of the hard state in the BH X-ray binary GX 339–4. We study its brightest hard-state observation by *XMM-Newton*, on 2010-03-28. We use the EPIC-pn data in the timing mode, fit the energy range of 0.7–10 keV and exclude the 1.75–2.35 keV range (to discard the range affected by calibration uncertainties), as in Basak & Zdziarski (2016). The *XMM-Newton* observation was accompanied by a contemporaneous observation by *RXTE*, for which only the PCA data are available. We fit jointly both data sets in order to better constrain the underlying slope of the spectrum and to estimate the total flux. However, as shown in Basak & Zdziarski (2016), there are significant differences in the residuals in the joint fit of these data. This appears to be due to the PCA spectral calibration being significantly different from that of the EPIC-pn at $E \lesssim 10$ keV, while the two are in good agreement at higher energies (see fig. 3 in Kolehmainen et al. 2014). Therefore, in our joint fit, we use the PCA data only at $E > 9$ keV. On the other hand, these data become very noisy at $E > 35$ keV, which we discard.

We fit the joint data by the model `tbabs(diskbb+reflkerr)`. The first component accounts for the ISM

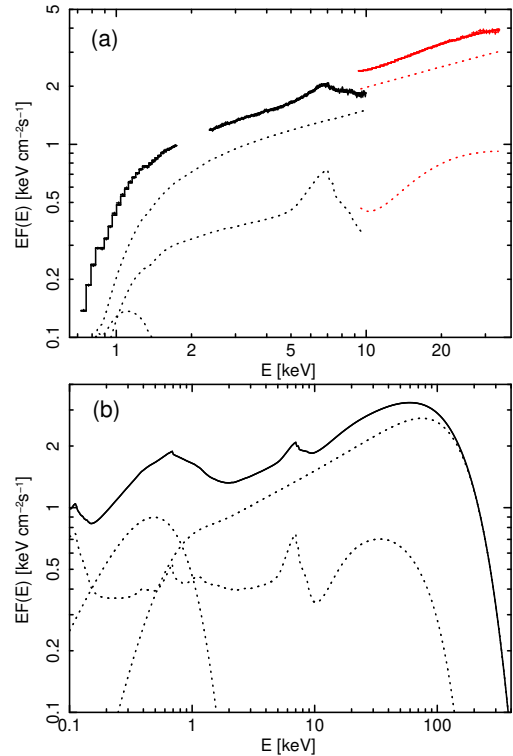


Figure 1. (a) The unfolded *XMM-Newton* and *RXTE* spectra. The dotted curves show the disk blackbody, the incident thermal Comptonization spectrum, and the reflected spectrum. (b) The unabsorbed model with the same components.

absorption (Wilms et al. 2000). The relativistic reflection model `reflkerr` (Niedźwiecki et al. 2019) assumes the thermal Comptonization model of Poutanen & Svensson (1996) as the incident spectrum, and we use the option `geom=0`, which corresponds to the primary source being isotropic in the local frame. We assume the dimensionless BH spin of $a_* = 0.998$, and the emissivity $\propto R^{-3}$. That model uses the static reflection model `xillver` (García et al. 2013), which assumes the reflector density of 10^{15} cm^{-3} . Considering also the fitted ionization parameter of $\xi \sim 10^3 \text{ erg cm s}^{-2}$ (Table 1), this implies a low irradiating flux (see Equation 6 below), at which the bulk of the reprocessed emission is at $\lesssim 0.1$ keV (cf. fig. 7 in García et al. 2016). The much higher F_{irr} of our fitted model implies the presence of a reprocessed soft component at higher energies. Reflection models suitable for high density ($> 10^{19} \text{ cm}^{-3}$) in the disk would be needed in order to self-consistently account for that. However, such models are currently not publicly available (Jiang et al. 2019a). Therefore, we use the `diskbb` disk blackbody model (Mitsuda et al. 1984) to approximate the reprocessed soft component, with the temperature of blackbody seed photons for Comptonization equal to that at the disk inner radius. These models are used within the X-ray fitting package `XSPEC` (Arnaud 1996).

Our fit results are given in Table 1, the unfolded spectrum together with the absorbed model is shown in Figure 1a and the unabsorbed model components are shown in Figure 1b.

Table 1. The results of the spectral fit with `tbabs (diskbb+reflkerr)`.

N_{H}	y	kT_e	R_{in}	Z_{Fe}	i	\mathcal{R}	$\log_{10} \xi$	N	kT_{in}	N_{disk}	A_{PCA}	χ^2/ν
10^{21} cm^{-2}		keV	R_{ISCO}		$^\circ$		erg cm s^{-1}		keV	10^4		
$7.4^{+0.2}_{-0.1}$	$1.25^{+0.01}_{-0.01}$	42^{+2}_{-3}	$12.4^{+2.7}_{-2.2}$	$4.9^{+0.1}_{-0.2}$	34^{+1}_{-2}	$0.28^{+0.01}_{-0.02}$	$3.40^{+0.02}_{-0.02}$	0.74	$0.207^{+0.003}_{-0.004}$	$7.2^{+0.3}_{-0.4}$	$1.31^{+0.01}_{-0.01}$	172/186

Note. $y \equiv 4\tau kT_e/m_e c^2$, $Z_{\text{Fe}} \leq 5$ is imposed, N is the flux density of `reflkerr` at 1 keV, $R_{\text{ISCO}}(a_* = 0.998) \approx 1.237R_g$, A_{PCA} is the relative PCA/EPIC-pn flux normalization. The uncertainties are for 90% confidence, $\Delta\chi^2 \approx 2.71$.

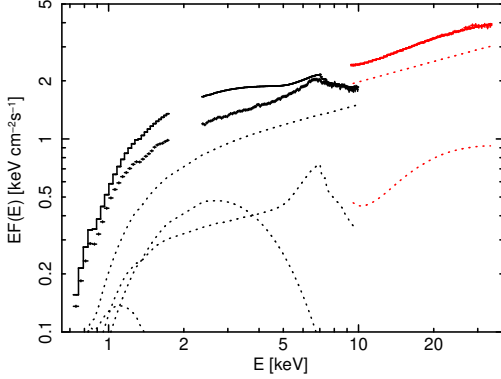


Figure 2. The unfolded *XMM-Newton* and *RXTE* spectra with the added disk blackbody component from irradiation with $kT_{\text{col,in}} = 1$ keV and $F_{\text{obs,disk}} = 1.7 \times 10^{-8} \text{ erg cm}^{-2} \text{ s}^{-1}$. The dotted curves show the two disk blackbodies, Comptonization and reflection.

We find a truncated disk, with $R_{\text{in}} \approx 15.3^{+3.4}_{-2.7} R_g$, and a low reflection fraction (defined as the ratio of the irradiating flux to that emitted outside in a local frame) of $\mathcal{R} \approx 0.28$. The fitted high reflector Fe abundance, Z_{Fe} , is probably an artefact of assuming a low disk density (e.g., Tomsick et al. 2018). The fitted electron temperature of $kT_e \approx 42$ keV is similar to the values found in high- L hard states of GX 339–4 by Wardziński et al. (2002), whose fits included the *CGRO/OSSE* data with significant source detection up to ≈ 500 keV, thus well constraining the actual value of kT_e .

We assume $M = 8M_\odot$, $D = 10$ kpc (see Heida et al. 2017 and model D2 of Zdziarski et al. 2019). The 0.1 – 10^3 keV total absorption-corrected flux of this model is $\approx 2.4 \times 10^{-8} \text{ erg cm}^{-2} \text{ s}^{-1}$, which corresponds to the isotropic luminosity of $L \approx 2.9 \times 10^{38} (D/10 \text{ kpc})^2 \text{ erg s}^{-1}$, and 24% of the Eddington luminosity at those M and D . We estimate the flux from the *XMM-Newton* data rather than from the PCA (which would yield the fluxes ≈ 1.3 times higher). The flux in the Comptonization component is $\approx 1.6 \times 10^{-8} \text{ erg cm}^{-2} \text{ s}^{-1}$. From comparing the incident and reflected/reprocessed components (and accounting for the low reflection fraction) in Figure 1b, we infer that the latter is dominated by back-scattering and Fe K fluorescence above ~ 1 – 2 keV, while below it is dominated by reemission of absorbed more-energetic photons. Thus, we calculate the albedo by comparing the incident and angle-averaged reflected fluxes at $E \geq 1$ keV, obtaining $a \approx 0.63$. This implies that the remaining flux has to be emitted as reprocessed emission at energies higher than those corresponding to kT_{eff} , see Equation (1).

We then consider how to account for the obtained low fractional reflection, $\mathcal{R} \approx 0.28$. One possibility is a reduction of the observed \mathcal{R} due to scattering in the corona (Steiner et al. 2017). We have tested this by Comptonizing a fraction, f_{sc} , of the reflected spectrum using the convolution model `ThComp` (Zdziarski et al. 2020). The best fit was at a negligible scattering fraction, and $f_{\text{sc}} \lesssim 0.02$ at 90% confidence. On the other hand, the fits to a spectrum from *RXTE* PCA averaged over a few outbursts of GX 339–4 by Steiner et al. (2017) using their code `simplcut` allowed $f_{\text{sc}} \lesssim 0.5$ with \mathcal{R} increasing then to ~ 1 . Thus, we consider this explanation still possible in principle. In that case, F_{irr} at the disk surface would be given by Equation (2).

Another possibility is that the primary source consists of two main parts; one forming a corona above the disk (and emitting $\sim 50\%$ toward it), and the other forming a hot flow inside the truncation radius, emitting mostly away from the disk, as for a partial overlap between hot and cold flows (cf. fig. 1f in Poutanen et al. 2018). The presence of the hot inner flow is supported by our fit with $R_{\text{in}} \gg R_{\text{ISCO}}$. Neglecting some complications associated with details of this geometry, we assume that a fraction \mathcal{R} of the primary luminosity, L_0 , is emitted by the corona, whose reflection is then observed, and the remainder is emitted by the hot inner flow, without any associated reflection. We thus multiply F_{irr} of Equation (2) by \mathcal{R} , which is a conservative choice, minimizing T_{eff} . We further assume $F_{\text{intr}} = 0$, and obtain,

$$T_{\text{eff,in}} \approx \left[\frac{2(1-a)\mathcal{R}F_{\text{obs},0}}{\sigma} \right]^{1/4} \left(\frac{D}{R_{\text{in}}} \right)^{1/2}, \quad (3)$$

$$\frac{kT_{\text{eff,in}}}{1 \text{ keV}} \approx 0.86 \left(\frac{R_{\text{in}}}{2R_g} \right)^{-1/2} \left(\frac{D}{10 \text{ kpc}} \right)^{1/2} \left(\frac{M}{8M_\odot} \right)^{-1/2}, \quad (4)$$

where Equation (4) corresponds to our data, scaling $T_{\text{eff,in}}$ to $R_{\text{in}} = 2R_g$ obtained by García et al. (2015) for similar states of GX 339–4. The corresponding color temperature is then $kT_{\text{col,in}} > 1$ keV. The observed disk blackbody flux in this component would then be

$$F_{\text{obs,disk}} \approx (1-a)\mathcal{R}F_{\text{obs},0}, \quad (5)$$

which is $\approx 1.7 \times 10^{-9} \text{ erg cm}^{-2} \text{ s}^{-1}$. In Figure 2, we simply added the disk blackbody component from the estimated irradiation, in order to illustrate its appearance. We have also fitted it to the data, by allowing the temperature and the flux of this component to be ≥ 1 keV, $\geq 1.7 \times 10^{-9} \text{ erg cm}^{-2} \text{ s}^{-1}$, respectively, tying the temperature of the seed photons for Comptonization to $T_{\text{col,in}}$ and allowing another disk blackbody at a lower temperature (which is strongly required by

the data). The obtained fit was very poor, with $\chi^2/\nu = 887/184$. Thus, the presence of such a high- T spectral component from irradiation appears to be completely ruled out by the data, even including all possible uncertainties in D , M , κ , and corrections for GR. This is also in agreement with previous fits of high-flux hard states of GX 339–4 (García et al. 2015; Basak & Zdziarski 2016; Dzielak et al. 2019), which showed no trace of such a component.

At our fitted $R_{\text{in}} \approx 15.3^{+3.4}_{-2.7} R_g$, $kT_{\text{eff,in}} \approx 0.28\text{--}0.34$ keV, which is still more than the allowed by the data, even for $\kappa = 1$. The above considerations then imply $R_{\text{in}} > 30R_g$, which, given the uncertainties intrinsic to spectral fitting, appears possible for the studied data.

3. THE DISK DENSITY

Another major constraint follows if both the ionization state and the density of the reflecting medium are known. The ionization parameter is defined as

$$\xi \equiv \frac{4\pi F'_{\text{irr}}}{n}, \quad (6)$$

where F'_{irr} is the irradiating flux measured at the source in either the 0.01–100 keV or 0.1–1000 keV photon energy ranges and n is either the H or electron density in the high-density reflection codes `reflionx` (Ross et al. 1999; Ross & Fabian 2007) and `relxillD` (García et al. 2016; J. García, private communication), respectively. Then, n and ξ can be fitted to data yielding $n = n_{\text{fit}}$ and its uncertainty, as done by Tomsick et al. (2018) and Jiang et al. (2019a,b). Here, we use results reported in those papers to check the self-consistency of their best-fit models, with the goal of being able to constrain R_{in} .

We follow Section 2 in relating the irradiating flux to the fitted direct component of the observed flux, $F_{\text{obs},0}$. As in the above-mentioned papers, we take the irradiating spectrum to be an exponentially cut-off power-law with a photon index, Γ , and a high-energy cutoff, E_{cut} , i.e., $dF/dE \propto E^{1-\Gamma} \exp(-E/E_{\text{cut}})$. $F_{\text{obs},0}$ can be then rescaled to the energy ranges used in either code using the fitted values of Γ and E_{cut} . We denote the rescaled observed direct flux by $F'_{\text{obs},0}$, and Equation (6) gives $n_{\text{cal}} = 16\pi^2 \mathcal{R} F'_{\text{obs},0} D^2 / (\zeta R^2 \xi)$. We then take $R = R_{\text{in}}$ as fitted to the observed reflection spectra using `reflionx` and `relxillD` with radial emissivity profiles, giving

$$n_{\text{cal}} = \frac{16\pi^2 \mathcal{R} F'_{\text{obs},0} (F_{\text{obs},0}, \Gamma, E_{\text{cut}}) D^2 c^4}{\zeta (R_{\text{in}}/R_{\text{ISCO}})^2 (R_{\text{ISCO}}/R_g)^2 M^2 G^2 \xi}, \quad (7)$$

where $\zeta = 2\pi$ for the emissivity $\propto R^{-3}$, and R_{ISCO} is a function of a_* (Bardeen et al. 1972).

The results for these calculations are shown in Figure 3, where we set $\mathcal{R} = 1$, following the assumption of the purely coronal geometry in Tomsick et al. (2018) and Jiang et al. (2019a,b), as well as because \mathcal{R} is not given in those papers. The magenta diagonal line corresponds to $n_{\text{cal}} = n_{\text{fit}}$ at $\zeta = 2\pi$. The uncertainties on n_{cal} are based on the uncertainties on the power-law flux, Γ , E_{cut} , ξ , $R_{\text{in}}/R_{\text{ISCO}}$, a_*

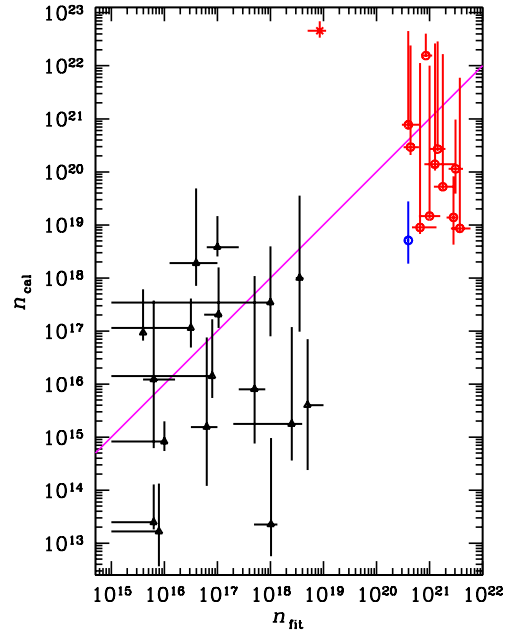


Figure 3. Comparison of the values of the density fitted by the reflection codes, n_{fit} , and those based on the irradiating flux assuming $\mathcal{R} = 1$, Equation (7). The magenta line shows $n_{\text{cal}} = n_{\text{fit}}$. The red symbols, blue open circle and black triangles (all with error bars) show the results for GX 339–4, Cyg X-1 and Seyferts fitted by Jiang et al. (2019a), Tomsick et al. (2018) and Jiang et al. (2019b), respectively. The red open squares and the cross correspond to the hard and very high state, respectively, of GX 339–4.

and M . Often, only upper or lower limits of some parameters are available. In those cases, we use the given limits in calculating the middle points of n_{cal} , which results in some error ranges being strongly asymmetric. We note that these parameters have often large uncertainties, of the order of the given best-fit quantity or larger. Therefore, we cannot use the standard propagation of errors, since it assumes the uncertainty to be much lower than the best-fit value. Instead, we estimate the uncertainties by calculating the maximum and minimum of n_{cal} corresponding to the extreme values of the parameters that maximize and minimize, respectively, its value. This method is conservative, i.e., it gives errors larger than those resulting from random scatter of the parameters.

The red points refer to the 12 observations of GX 339–4 studied by Jiang et al. (2019a) using `reflionx` convolved with `relconv` (Dauser et al. 2016), assuming $a_* = 0.998$. We assume $M = 8M_{\odot}$ and $D = 10$ kpc; uncertainties on them and on \mathcal{R} and ζ can be accounted for by rescaling n_{cal} by a factor $\mathcal{R}D^2/(\zeta M^2)$. The points correspond to 11 observations in the low-flux hard state and one in the high-flux very high state (studied before by Parker et al. 2016). We see that, at $\mathcal{R} = 1$, most of the hard-state values of n_{cal} are compatible with being equal to n_{fit} within the error bars. The only clearly discrepant point with small error bars is the one characterized by the highest value of n_{cal} for the hard state (LF10 in Jiang et al. 2019a), for which

$R_{\text{in}} < 1.51R_{\text{ISCO}}$ was reported, while $R_{\text{in}} \lesssim (5-30)R_{\text{ISCO}}$ were found for the remaining 10 hard-state observations. At the face value, this overall agreement would support the accuracy of the latter estimates.

On the other hand, the very high state observation has small error bars and $n_{\text{cal}} \approx 5400n_{\text{fit}}$ at the assumed $R_{\text{in}} = R_{\text{ISCO}}$. This discrepancy between n_{cal} and n_{fit} could be removed if $(\zeta/2\pi)^{1/2}(R_{\text{in}}/R_{\text{ISCO}})(M/8M_{\odot})(10\text{ kpc}/D) \approx 70$, which appears unlikely. A possible explanation of this discrepancy is the adopted assumption of a passive accretion disk. It may be approximately correct for the hard state, where most of the luminosity is emitted by the corona, but it is certainly not proper for the soft state, where the dominant disk intrinsic dissipation emitted as a color-corrected blackbody is compatible with the emitted spectrum.

The blue data point corresponds to the observation of the BH binary Cyg X-1 analyzed by Tomsick et al. (2018). We assume $M = 15M_{\odot}$, $D = 2\text{ kpc}$, and use the fit with the power-law emissivity given in their table 3. We note that their value of the power-law normalization is an order of magnitude above the value seen on their fig. 6. Here we use the latter. We find $n_{\text{cal}} \lesssim 0.15n_{\text{fit}}$, which discrepancy appears to be due to some systematic errors of the used methods.

We finally include the results obtained for 17 Seyfert galaxies by Jiang et al. (2019b); see the black points in Figure 3. Here, $R_{\text{in}} = R_{\text{ISCO}}$ is assumed, a_* is fitted, the distances are based on the redshift for $H_0 = 73\text{ km s}^{-1}\text{ Mpc}^{-1}$, and `relxillD` is used. We see a very large scatter, indicating problems with some of the assumptions and/or methods.

We then check the validity and self-consistency of the assumption of $\mathcal{R} = 1$. While the best-fit values of \mathcal{R} are not reported in Jiang et al. (2019a), they can be approximately inferred from their fig. 6 as the ratio of the relativistic reflection component to the power-law one in the range of 10–30 keV. The resulting values are $\mathcal{R} \approx 0.02-0.05$ in all hard-state cases except observation LF1, where we infer $\mathcal{R} \approx 0.15$, i.e., are all $\ll 1$. Based on those values, we found from Equations (3), (5) that the low-energy spectral features present in those fits are consistent with our estimates of the quasi-thermal re-radiation of the incident emission, as expected considering that a high-density reflection model was used in those fits. However, this agreement is largely a consequence of including rather luminous distant (not relativistically broadened) reflection component. Such component in all of the cases is either as strong or stronger than the relativistic component. Therefore, the inner disk becomes weakly irradiated, thus explaining the weakness of the quasi-thermal components in the observed spectra. However, that dominance of distant reflection strongly differs from the previous results of X-ray fitting of the hard state of GX 339–4 (García et al. 2015; Basak & Zdziarski 2016; Wang-Ji et al. 2018; Dzielak et al. 2019), where the distant reflection contributions were always significantly weaker than those of the close ones. Also, it appears not to be consistent with the assumed coronal geometry. In the high-flux state of GX 339–4, no distant reflection was included and we have estimated $\mathcal{R} \approx 1$. Thus, our result of $n_{\text{cal}} \gg n_{\text{fit}}$ in that case remains valid.

The above consideration shows that the values of n_{cal} of Equation (7) can be significantly overestimated if $\mathcal{R} = 1$ is assumed, especially in the case of the hard state GX 339–4. A more rigorous treatment would require considering the exact best-fit values of \mathcal{R} , which we do not know. Thus, the values of n_{cal} shown in Figure 3 (except for the point for the very high state of GX 339–4) should be considered as upper limits, and the apparent overall agreement for the hard state of GX 339–4 may be spurious.

4. DISCUSSION AND CONCLUSIONS

We have derived a powerful method constraining the inner radii of accretion disks in accreting BH binaries based on the Stefan-Boltzmann law, $F_{\text{irr}} = \sigma T_{\text{eff}}^4$. The constraint follows from considering the flux irradiating the innermost parts of the disk, which requires the presence of a quasi-thermal component at a color temperature higher than T_{eff} associated with the Fe K and reflection components. The absence of this component with $kT_{\text{col}} \sim 1\text{ keV}$ in the data completely rules out the presence of a disk extending close to the ISCO in high-luminosity hard states, e.g., in GX 339–4. This constraint has been overlooked before owing to the wide-spread use of reflection codes assuming low density and fitting the ionization parameter, $\xi \propto F_{\text{irr}}/n$, which implicitly yields F_{irr} much below the fluxes typical for the luminous hard state, and consequently the effective temperatures of the irradiated media having values consistent with the observations even at $R_{\text{in}} \approx R_{\text{ISCO}}$.

We have derived the above constraint by conservatively assuming that the disc is irradiated only by a small fraction of the primary flux, which is the case if there is a hot inner flow at $R < R_{\text{in}}$. In the pure coronal geometry, the irradiating flux at the disk surface is higher, making the constraint stronger. The constraint is also very strong in the geometry of a lamp-post surrounded by a disk extending close to the ISCO, where the bare disk is irradiated by gravitationally focused primary radiation. Our constraint requires the truncated disk geometry in luminous hard states, supporting, among others, the findings based on the energy balance (Poutanen et al. 2018) and on comprehensive modelling of both the spectral and timing features (Mahmoud et al. 2019).

The constraint becomes weaker at lower luminosities. But given the slow dependence of $T_{\text{eff}} \propto F_{\text{irr}}^{1/4}$, it is still quite powerful at L of the order of a per cent of the Eddington luminosity in BH binaries. The strict application of our formalism in the future would require an availability of a public reflection code valid at densities $> 10^{19}\text{ cm}^{-3}$. In the Seyfert case, the thermal feature from the irradiation occurs in the UV range. Still, it is highly desirable to study the resulting constraints given the evidence for the disks extending close to the ISCO in those systems (e.g., De Marco et al. 2013).

In the second part of the paper, we have derived a method based on comparing the disk densities fitted (by other authors) using high-density reflection codes with those calculated by us from $n \propto \xi F_{\text{irr}}$ using the fitted ionization parameter, the source luminosity and the disk inner radius. However, we have found a very large scatter of the density ratios, pre-

venting us from obtaining significant constraints on the disk inner radius as yet. In the high-luminosity very high state of GX 339–4, where the assumed $R_{\text{in}} \approx R_{\text{ISCO}}$ is likely, the fitted density was much too low to be self-consistent. A possible explanation for that is the used method assumed a passive disk while strong internal dissipation is present in that state. It is clear that more work is required to achieve a reasonable sensitivity of this method in constraining R_{in} .

ACKNOWLEDGMENTS

We thank J. García, J. Jiang, A. Niedźwiecki and M. Sza-necki for valuable discussions. We have benefitted from discussions during Team Meetings of the International Space Science Institute in Bern, whose support we acknowledge. We also acknowledge support from the Polish National Science Centre under the grant 2015/18/A/ST9/00746 and the European Union’s Horizon 2020 research and innovation programme under the Marie Skłodowska-Curie grant agreement No. 798726.

REFERENCES

- Arnaud, K. A. 1996, *Astronomical Society of the Pacific Conference Series*, Vol. 101, *XSPEC: The First Ten Years*, ed. G. H. Jacoby & J. Barnes, 17
- Bardeen, J. M., Press, W. H., & Teukolsky, S. A. 1972, *ApJ*, 178, 347, doi: [10.1086/151796](https://doi.org/10.1086/151796)
- Basak, R., & Zdziarski, A. A. 2016, *MNRAS*, 458, 2199, doi: [10.1093/mnras/stw420](https://doi.org/10.1093/mnras/stw420)
- Bernardini, F., Russell, D. M., Shaw, A. W., et al. 2016, *ApJL*, 818, L5, doi: [10.3847/2041-8205/818/1/L5](https://doi.org/10.3847/2041-8205/818/1/L5)
- Dauser, T., García, J., Walton, D. J., et al. 2016, *A&A*, 590, A76, doi: [10.1051/0004-6361/201628135](https://doi.org/10.1051/0004-6361/201628135)
- Davis, S. W., Blaes, O. M., Hubeny, I., & Turner, N. J. 2005, *ApJ*, 621, 372, doi: [10.1086/427278](https://doi.org/10.1086/427278)
- De Marco, B., Ponti, G., Cappi, M., et al. 2013, *MNRAS*, 431, 2441, doi: [10.1093/mnras/stt339](https://doi.org/10.1093/mnras/stt339)
- Dubus, G., Hameury, J.-M., & Lasota, J.-P. 2001, *A&A*, 373, 251, doi: [10.1051/0004-6361:20010632](https://doi.org/10.1051/0004-6361:20010632)
- Dzielałak, M. A., Zdziarski, A. A., Szanecki, M., et al. 2019, *MNRAS*, 485, 3845, doi: [10.1093/mnras/stz668](https://doi.org/10.1093/mnras/stz668)
- García, J., Dauser, T., Reynolds, C. S., et al. 2013, *ApJ*, 768, 146, doi: [10.1088/0004-637X/768/2/146](https://doi.org/10.1088/0004-637X/768/2/146)
- García, J. A., Fabian, A. C., Kallman, T. R., et al. 2016, *MNRAS*, 462, 751, doi: [10.1093/mnras/stw1696](https://doi.org/10.1093/mnras/stw1696)
- García, J. A., Steiner, J. F., McClintock, J. E., et al. 2015, *ApJ*, 813, 84, doi: [10.1088/0004-637X/813/2/84](https://doi.org/10.1088/0004-637X/813/2/84)
- Heida, M., Jonker, P. G., Torres, M. A. P., & Chiavassa, A. 2017, *ApJ*, 846, 132, doi: [10.3847/1538-4357/aa85df](https://doi.org/10.3847/1538-4357/aa85df)
- Jiang, J., Fabian, A. C., Wang, J., et al. 2019a, *MNRAS*, 484, 1972, doi: [10.1093/mnras/stz095](https://doi.org/10.1093/mnras/stz095)
- Jiang, J., Fabian, A. C., Dauser, T., et al. 2019b, *MNRAS*, 489, 3436, doi: [10.1093/mnras/stz2326](https://doi.org/10.1093/mnras/stz2326)
- Kara, E., Steiner, J. F., Fabian, A. C., et al. 2019, *Nature*, 565, 198, doi: [10.1038/s41586-018-0803-x](https://doi.org/10.1038/s41586-018-0803-x)
- Kolehmainen, M., Done, C., & Díaz Trigo, M. 2014, *MNRAS*, 437, 316, doi: [10.1093/mnras/st1886](https://doi.org/10.1093/mnras/st1886)
- Mahmoud, R. D., Done, C., & De Marco, B. 2019, *MNRAS*, 486, 2137, doi: [10.1093/mnras/stz933](https://doi.org/10.1093/mnras/stz933)
- Mitsuda, K., Inoue, H., Koyama, K., et al. 1984, *PASJ*, 36, 741
- Niedźwiecki, A., Szanecki, M., & Zdziarski, A. A. 2019, *MNRAS*, 485, 2942, doi: [10.1093/mnras/stz487](https://doi.org/10.1093/mnras/stz487)
- Parker, M. L., Tomsick, J. A., Kennea, J. A., et al. 2016, *ApJL*, 821, L6, doi: [10.3847/2041-8205/821/1/L6](https://doi.org/10.3847/2041-8205/821/1/L6)
- Poutanen, J., & Svensson, R. 1996, *ApJ*, 470, 249, doi: [10.1086/177865](https://doi.org/10.1086/177865)
- Poutanen, J., Veledina, A., & Zdziarski, A. A. 2018, *A&A*, 614, A79, doi: [10.1051/0004-6361/201732345](https://doi.org/10.1051/0004-6361/201732345)
- Ross, R. R., & Fabian, A. C. 2007, *MNRAS*, 381, 1697, doi: [10.1111/j.1365-2966.2007.12339.x](https://doi.org/10.1111/j.1365-2966.2007.12339.x)
- Ross, R. R., Fabian, A. C., & Young, A. J. 1999, *MNRAS*, 306, 461, doi: [10.1046/j.1365-8711.1999.02528.x](https://doi.org/10.1046/j.1365-8711.1999.02528.x)
- Shimura, T., & Takahara, F. 1995, *ApJ*, 445, 780, doi: [10.1086/175740](https://doi.org/10.1086/175740)
- Steiner, J. F., García, J. A., Eikmann, W., et al. 2017, *ApJ*, 836, 119, doi: [10.3847/1538-4357/836/1/119](https://doi.org/10.3847/1538-4357/836/1/119)
- Tomsick, J. A., Parker, M. L., García, J. A., et al. 2018, *ApJ*, 855, 3, doi: [10.3847/1538-4357/aaaab1](https://doi.org/10.3847/1538-4357/aaaab1)
- Wang-Ji, J., García, J. A., Steiner, J. F., et al. 2018, *ApJ*, 855, 61, doi: [10.3847/1538-4357/aaa974](https://doi.org/10.3847/1538-4357/aaa974)
- Wardziński, G., Zdziarski, A. A., Gierliński, M., et al. 2002, *MNRAS*, 337, 829, doi: [10.1046/j.1365-8711.2002.05914.x](https://doi.org/10.1046/j.1365-8711.2002.05914.x)
- Wilms, J., Allen, A., & McCray, R. 2000, *ApJ*, 542, 914, doi: [10.1086/317016](https://doi.org/10.1086/317016)
- Yuan, F., & Narayan, R. 2014, *ARA&A*, 52, 529, doi: [10.1146/annurev-astro-082812-141003](https://doi.org/10.1146/annurev-astro-082812-141003)
- Zdziarski, A. A., Szanecki, M., Poutanen, J., Gierliński, M., & Biernacki, P. 2020, *MNRAS*, doi: [10.1093/mnras/staa159](https://doi.org/10.1093/mnras/staa159)
- Zdziarski, A. A., Ziółkowski, J., & Mikołajewska, J. 2019, *MNRAS*, 488, 1026, doi: [10.1093/mnras/stz1787](https://doi.org/10.1093/mnras/stz1787)